Chapter XXVIII: Dosimetry – Physical

Ke Sheng, Ph.D.

Department of Radiation Oncology

University of California, Los Angeles

Background

Preclinical studies are essential to test hypotheses in biological research. It is also an important step to validate the efficacy of a treatment before they can be used on human patients. Radiobiology is one of the fields that can particularly benefit from preclinical research. Due to the risk associated with ionizing radiation, new treatment involving this modality, either to use or to mitigate it, will have to go through rigorous tests on animal models before it may be tested in human clinical trials. In some cases, such as mitigation of radiation toxicities from the nuclear disasters, a prospective clinical trial may not even be possible, and animal studies are the only way to test the effectiveness of compounds mitigating the radiation damage. On the other hand, there is a risk that a treatment tested effective in a particular preclinical setting may not always be effective on human patients. In fact, the reproducibility of preclinical results themselves has been a paramount challenge, which has risen to be an intense focus in recent years[1,2]. It has been estimated that between 51% and 89% of the preclinical studies are not reproducible[4]. Center for Open Science and Science Exchange launched a project to examine the reproducibility of high-profile cancer research and the early results are mixed [5]. There are many factors that can contribute to the low reproducibility of preclinical research results. Variability in the biological systems, the authenticity of chemical agents, experimental conditions, contaminations, adherence to the standard operating procedures all can influence the results. In the case radiobiology studies, radiation dosimetry is another variable that has a profound impact. Irreproducible studies not only can delay the development of cure that the patients desperately need but also cause a huge economic waste[6]. The reproducibility of preclinical studies depends on if all factors contributing to the results are individually accurate. Specifically, for radiobiological experiments, the accuracy of radiation dosimetry is pivotal.

Compared to chemical agents with complicated pharmacokinetics and molecular pathways, radiation dose delivery may appear to be highly quantifiable. This statement is mostly true in human radiotherapy. In the past decades, rigorous dosimetry standard has been established and practiced in radiation oncology. Except for isolated incidents, the human radiation delivery in the developed countries has been considered accurate, resulting in overall safe practice with reproducible dose constraints that most agree on. Unfortunately, the success of human radiation therapy cannot be easily translated to preclinical studies due to multiple reasons. First, the modern accuracy of radiation therapy is established on massive investment in equipment and personnel. Human radiation therapy machines are designed to achieve 2% dosimetric accuracy. These machines are being regularly maintained and then replaced typically every 10-15 years. Self-check mechanisms are mandatory for human radiation therapy machines to ensure dosimetric feedback. These machines are quality-assured daily by trained staff. More rigorous mechanical accuracy and dosimetric output checks are performed on a monthly and annual basis by certified medical physicists using equipment with calibration traceable to NIST. At the cross-institutional level, both the machine output and patient-specific plan delivery are being independently checked by centralized services to ensure consistency and inter-comparability[7]. The service is provided by NCI funded Imaging and Radiation Oncology Core (IROC). In comparison, the amount of technological and human resources for preclinical irradiation procedures is severely constrained. Many older irradiators are still in service, most without a dosimetric feedback mechanism, i.e., other than a timer, there is no indication of the actual dose delivery on these systems. Both the frequency and quality of machine QA are inadequate to ensure the high accuracy of radiation delivery. Dedicated medical physicists for preclinical irradiation are rare, not to mention systematic training and certification for these positions. Second, human treatment machines are more homogeneous than preclinical irradiators, which are diverse in both treatment geometry and type of radiation sources, which can be X-ray tubes, accelerators or isotopes, making it impractical to standardize and simplify the QA protocols. Third, sophisticated computational models are established for human treatment machines. These models are commissioned using actual measurement data and then used to calculate 3D dose distribution for patients based on patient computed tomography (CT) and other 3D medical images. To further reduce inter-operator inconsistency, in recent years, knowledge-based treatment planning has been developed to make treatment planning for human patients even more reproducible and consistent[8,9]. Additional measurements are commonly performed for individual patients and plans. In contrast, most preclinical irradiators only have a look-up table to estimate a point dose that does not fully represent the

volume dose received by the animals. Radiation physics of small animals is fundamentally more challenging than human irradiation. For the size of mice, electron equilibrium condition, which is essential for simple dose prediction without resorting to more complex calculation methods such as Monte Carlo, is not satisfied when MV sources are used for treatment. On the other hand, kV X-rays are sensitive to the material properties, making the convenient assumption of water equivalence for various tissue types inaccurate. Chow et al. using Monte Carlo calculations for 100 kV and 225 kV x-ray beams, demonstrated that mouse bone had over 400 % greater dose than that in water or soft tissue[10]. Further challenges are from the setup accuracy. Different from patient treatment where the patient positioning is guided by not only room lasers but also 2D and 3D images, animal set up are often cruder without accurately determining the distance from the animal to the radiation source. Due to less robust immobilization, the distance in treatment may not be held constant. Because the treatment distance on a typical X-ray machine is approximately 30-50% of that of the human treatment machine, one centimeter of set up error in the beam direction alone could contribute to up to 4-10% dose errors due to beam divergence.

Recognizing the paramount challenges in preclinical radiation dosimetry accuracy and consistency, stake holders have begun working to address the challenges. In September of 2011, the National Cancer Institute (NCI), the National Institute of Allergy and Infectious Diseases (NIAID), and the National Institute of Standards and Technology (NIST) organized a workshop including representatives of the radiobiology and radiation physics communities[11]. They have identified many causes that may have contributed to the preclinical irradiation uncertainties. One area that was particularly worth noting besides the actual machine and dosimetric calibration is the lack of reported details in radiobiological studies. For a study to be reproduced, the following four categories of information are needed:

1. Radiation field(s) to be used (e.g., radiation output, uniformity, energy)
2. Absorbed dose throughout the biological subject
3. Dose uniformity within the subject
4. Reproducibility of dose across a study group

A survey of papers published between 2010 and 2011 in the Journal of Radiation Research found that only 7% of them provided sufficient information for other labs to reproduce[11].

Related to this concerted effort to improve dosimetric consistency, Centers for Medical Countermeasures against Radiation (CMCR) established by National Institute of Allergy and Infectious Diseases (NIAID) is particularly worth noting[12]. CMCR was established as the aftermath of 9/11 terrorism attack. Due to the risk of radiation exposure for potential attacks, it was important to develop compounds that can drastically reduce the radiation toxicity and maximally protect human lives should such events happen. The efficacy is quantified by reduction of tissue damage or animal lethality at the same radiation dose level to the same tissue volume and should be consistent across participating centers.

In this book chapter, the individual causes to the dosimetric inaccuracies are analyzed and potential solutions presented.

Current preclinical irradiator survey results

Several surveys have been conducted to gauge the accuracy of preclinical radiation. Pedersen et al[13] conducted a survey of irradiator output verification study of 12 radiation biology laboratories (7 gamma and 5 X-ray units) using polymethyl methacrylate (PMMA) mouse phantoms and thermoluminescent dosimeters (TLDs) readouts at the University of Wisconsin Medical Radiation Research Center (UWMRRC). The laboratories housing each of these irradiators were asked to deliver specific doses to individual mouse phantoms. Simultaneously, mouse phantoms at the UWMRRC were irradiated with NIST-traceable reference beams representative of the subject laboratories' beam energies. The irradiated mouse phantoms were returned from the various institutions to the UWMRRC and the TLDs were processed, with their measured dose-response compared to the known dose response of the calibration phantom TLDs. The results show a relatively acceptable output for the 137 Cs irradiator but only one out of the five facilities using X-ray irradiators delivered an output within 5% of the target dose. The dose differences for the other four X-ray irradiators ranged from 12 to 42%.

Table 1. Radiation output survey results for 12 preclinical irradiators ([13])

Facility	***Source***	***Average of Measured Dose***		***Average %Deviation***
		1 Gy ADW	***4 Gy ADW***	
1	***^{137}Cs***	***1.12***	***4.41***	***11.2***

2	***^{137}Cs***	***1.09***	***4.32***	***8.7***
3	***^{137}Cs***	***1.06***	***4.12***	***3.9[a]***
4	***^{137}Cs***	***1.15***	***4.48***	***13.5***
5	***^{137}Cs***	***1.01***	***4.09***	***1.6***
6	***^{137}Cs***	***1.03***	***4.02***	***1.8***
7	***^{60}Co***	***1.02***	***4.08***	***1.8***
8	***X-ray 1***	***1.17***		***-12.4[b]***
9	***X-ray 2***	***0.838***	***3.39***	***-15.7***
10	***X-ray 3***	***0.580***	***2.07***	***-42.3***
11	***X-ray 4***	***0.986***	***3.99***	***-0.9***
12	***X-ray 5***	***0.826***	***3.51***	***-14.8***

The contrast between isotope irradiators and X-ray irradiators is understandable. Both the output and the energy of isotope irradiators are exactly known, leaving the only major variable to set up position. For Cs-137, up to 25% dose variation can still exist depending the location of exposure[14,15]. However, for the survey measurement, it is typical to place the dosimeter at a fixed location consistent to calibration condition. On the other hand, there are large uncertainties in the X-ray machine output and energy. Figure 1 shows the X-ray tube output decline over the course of 2 years. Since the decline is related to the tube condition and usage, there is not a universal trend that can be applied to all X-ray machines in contrast to the decay table of isotopes.

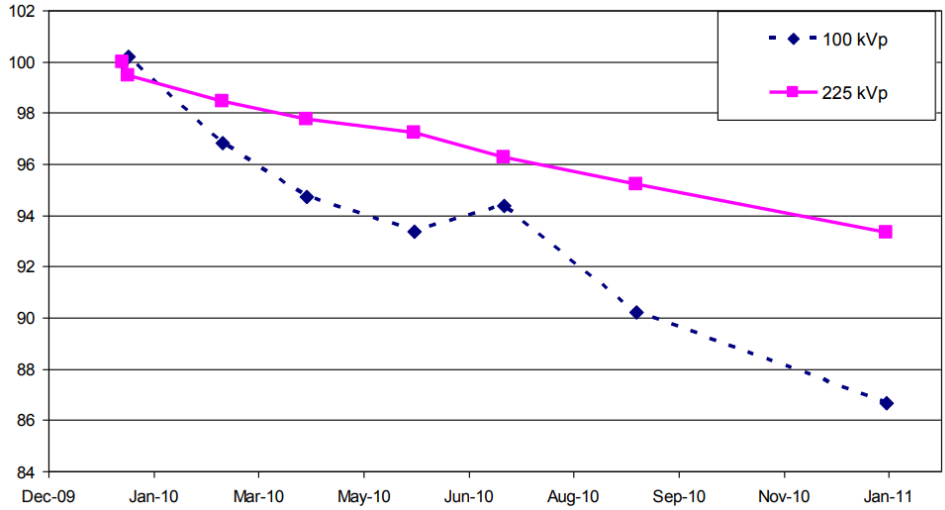

Figure 1. X-ray tube output over time (Courtesy Dr. Patricia Lindsay) of a preclinical irradiator (PXI cx225).

Machine-Specific QA Procedures

X-Ray Machines:

Typical x-ray irradiators operate in the range of 40-350 kVp using multiple filters (i.e., aluminum or copper), and an adjustable SSD from 20–90 cm. The most common nominal energy used for animal irradiation is higher than 225 kVp for tissue penetration and more uniform dose through the animals as small as nude mice. Output measurements from x-ray irradiators require knowledge of the half-value-layer (HVL) based on AAPM task group report TG-61[16]. TG-61 is a dosimetry protocol designed for low- and medium-energy external beam x-ray systems with tube potentials ranging between 40 and 350 kV, which covers the energy of typical preclinical X-ray irradiators. An ionization chamber is used to measure air kerma, K_{air}, which is converted to a dose to water using multiplicative correction factors [16]. With the X-ray tubes, the

electrons emitted from the cathode are accelerated by the electric field before hitting the anode, where the X-ray is produced via the bremsstrahlung effect. The resultant X-rays are not monochromatic. Instead, the X-rays photons are spread in a spectrum, which depends on the anode material and is subject to further modification by any filtration along the X-ray beam path. The HVL serves as a proxy for x-ray beam quality and is used to determine appropriate air-kerma calibration factors and mass energy absorption coefficients for conversion from air-kerma to absorbed tissue dose. HVL is measured using attenuator material (99.9% purity copper layers) on the beam path before a diaphragm. The thickness measurement accuracy is 0.05 mm. Although the standard copper sheet set for kV X-ray HVL measurement can be purchased from several vendors, this additional cost and knowledge to use them create a barrier for many preclinical facilities to determine if their system energy is within the intended range. What makes the X-ray systems more confusing to use is that typically multiple filters are available. Different combinations of aluminum, copper, and tin are used to modify the beam spectra for imaging or therapy applications at varying depths. These different filters not only change the energy but also substantially the output. For instance, on the image guided small animal irradiators, the copper filter is intended for 225 kVp therapy beam and the aluminum filter is intended for the 100 kVp or lower imaging beams. If the aluminum filter was mistakenly used for the 225 kVp beam, not only the effective energy would be significantly lower, the surface dose can be more than 100% higher, producing undesired skin toxicities on animals. Therefore, for a shared piece of instrument with removeable filters, fail to understand and correctly apply the filters can adversely impact the experimental results. An inexpensive and easy to use energy measurement kit is needed to help quantification and quality assure the kV X-ray unit energies. For absolute calibration, the raw ion chamber read will be corrected using the American Association of Physicists in Medicine (AAPM) protocol for 40–300 kV x-ray beam dosimetry in radiotherapy and radiobiology, which is also known as TG-61.

TG-61 and its limitation in the preclinical irradiation

TG-61 provides a framework for calibrating the X-ray machines for both human radiation therapy and small animal irradiation. It specifies two different calibration methods, one in-air the other in phantom. By placing the air chamber and the calibration point without any build up, the measurement, after corrections, indicates the surface dose. While placing the ion chamber in the phantom, the measurement is suited for determining the dose at a depth. However, it is important to note that TG-61 is biased towards measurement conditions in human treatment, which has important differences from the small animal irradiation. TG-61 calibration is based on so-called "narrow (good) beam geometry" with which the beams are collimated down to 20 cm diameter or smaller at the treatment distance while in many preclinical irradiation settings the X-ray beams are open without collimation due both to the lack of collimators on many existing X-ray machines, and that the practical need to treat many animals simultaneously. This resulted in three potential problems. First, there are no published correction coefficients for such wide fields. Since the backscatter factor increases steeply with the field size, without reliable correction coefficient, the ion chamber measured air kerma cannot be converted to surface dose. Second, the field inhomogeneity becomes more non-negligible for larger fields. The animals treated at the edge of a wide field could receive 20% lower dose than the animals treated at the center. Third, for human applications, TG-61 assumes that the radiation fields smaller than the irradiated medium for semi-infinite geometry. This condition is not met with small animal irradiation. Last, the scatter photon and electron contamination from the X-ray cabinet is increasingly influencing the dose with larger fields. These deviations from the idealized measurement condition specified in TG-61 resulted in inaccurately predicted dose in small animals. In an experiment conducted by Abogunde et al., it was shown that the calibration determined by TG-61 under-estimates the dose delivered to a mouse phantom by 3-7% compared with embedded MOSFET dosimeters (presentation entitled Dose Comparison between AAPM TG-61 protocol and MOSFET-based Phantom Dosimetry.)

Therefore, TG-61 is useful for point output determination and machine consistency check but there is a substantial gap between TG-61 and the dose actually received by the animals. In order to do so, it is necessary to combine TG-61 with in vivo dosimetry measurement specific to the project research protocols.

Cs-137 Irradiator:

Cs-137 has a half-life of 30.17 years; it decays via ^{137m}Ba to ^{137} Ba producing γ-ray with an average energy of 662 KeV. The Mark I-68A (JL Shepherd and Associates, San Fernando, CA) and GammaCell (Best Medical) 137Cs gamma irradiators shown in Figure 2, are two of commonly used Cs-137 irradiators. Despite the common radiation source, the two systems are markedly different in operation geometry. The Cs source rises from the safe and irradiate from inside out in the former while in the latter, the two Cs sources are static with the irradiation chamber moving between the sources for irradiation. Commercially available ^{137}Cs irradiator comes two main configurations: 1) with two fixed sources above and below the

irradiation volume and 2) with a translatable source central to the irradiation volume. Brady et al. provided an updated Cs-137 characterization using modern dosimetric tools[17].

Figure 2. A. Mark I-68A Cs-137 irradiator. B. Best GammaCell-40 Cs-137 irradiator stock photo.

These are the key parameters to achieve accurate dosimetry for Cs-137 irradiator: (a) Initial dose rate (output), (b) the isodose map, (c) dose rate measurements for specific experimental set-ups, (d) correction of the reference dose rate for radioactive decay, and (e) periodic quality assurance plan.

a) ***Initial Dose Rate.*** Initial dose rates are usually given by the manufacturer at the time of purchase and should be verified independently. The ATP dose rate will be checked against manufacture value, any finding from the ATP should be reviewed based on the pre-established criteria by the physicist. If the performance falls below acceptable standards, corrective actions should be taken to achieve proper and expected device performance.

b) ***The Methodology of Dose Rate Measurement.*** Given the geometry of the irradiator, the accuracy of dose delivery is also related to the methodology employed to measure the dose rate. Due to the rotational motion of the sample (to deliver uniform dose distribution to the small sample), the samples are exposed to different dose rates. The dose rate can be characterized as a function of the distance (d) from the source as $1/d^2$ law of radiation propagation at time *t* during irradiation different points. In fact, the samples are exposed to an average dose rate over the area traversed during irradiation. The dose rates for both stationary and rotation setup will be monitored on a monthly basis using the TLDs provided by the RPC.

c) ***Annual Dose Rate Decay Correction:*** The annual dose rate correction (decrease) is 2.3%, specifically the decay correction of 0.977 should be applied to the reference calibrated dose rate on yearly basis. An annual TLD irradiation service will be provided by the RPC[17].c. Annual dose rate decay correction: The annual dose rate correction (decrease) is 2.3%, specifically the decay correction of 0.977 should be applied to the reference calibrated dose rate on yearly basis. An annual TLD irradiation service will be provided by the RPC[17].

d) ***Timer Error.*** There is a finite error in source output measurements due to the source travel time from "off" to "on" and return. This time error should be included in calibration and spot-check measurements. There is a short period of time at the beginning and at the end of each irradiation when the exposure rate rises from zero (source fully shielded in "off" position) to a constant value (source fully "on") and then returns to zero. The radiation detector "sees" a variable portion of the source during the travel time but the timer mechanism is tripped only at a definite point in this travel. Hence, the length of time of source travel is reflected in the time error measurement. The timer error will be determined using the method described in Ref [18].

<u>Co-60:</u>

Co-60 is a synthetic radioactive isotope of cobalt with a half-life of 5.2714 years. It is produced artificially by neutron activation of the isotope Co-59. Co-60 decays by beta decay to the stable isotope nickel-60. The activated nickel nucleus emits two gamma rays with energies of 1.17 and 1.33 MeV with a mean energy of 1.25 MeV. Co-60 irradiators serve as a dosimetry standard in the radiation physics community and Co-60 represents the common calibration endpoint for ionization chambers used in radiotherapy. Current Co-60 machines used from preclinical studies are typically retired clinical machines. They are useful when larger animals are involved in the project due to its larger clearance and higher beam energy. The QA protocol for Co-60 machines was specified by American National Standards Institute in "Procedures for Periodic Inspection of Cobalt-60 and Cesium-137 Teletherapy Equipment"[18]. With update to original methodology using new equipment, pertinent quality check items include:

a) Light-Radiation-Field Congruence that can be checked using the GafChromic film

b) Determination of the machine output at a reference field size and depth in phantom using the Presage 3D dosimeter
c) Mechanical and radiation isocenter using GafChromic film (Star shots)
d) Output variation as a function of jaw size using ion chamber measurement
e) Source to subject distance by comparing the optical system and the front pointer
f) Determination of field uniformity across irradiation field sizes using GafChromic film
g) Timer error as described in the previous section for Cs-137
h) In addition to these QA measures, a monthly decay dose rate correction table should be established for monthly double check

Figure 3. Co-60 system (Philips XK 5101) used for rat irradiation[19].

Radioisotopes are advantageous in their highly predictable output but there is a trend to gradually phase them out for the safer X-ray and linear accelerator machines. For instance, there is an ongoing plan by the US National Nuclear Security Administration to replace all isotope machines for preclinical radiobiological experiments[20]. In California, there is a similar initiative to replace all Cs-137 irradiators with safer X-ray irradiators[21]. Cs-137 chloride is considered particularly dangerous because it is water-soluble, highly dispersible, relatively easy to shield and conceal, has a long half-life (~30 years) and high specific activity. Therefore, moving forward, the harmonization of preclinical dosimetry will need to shift its focus more towards the X-ray machines.

Dosimeters for the preclinical irradiator output measurement

There is a variety of dosimeters that can be potentially used for preclinical irradiation dose measurement. The joint NIST, NCI and NIAID workshop report [11] provides a list of dosimeters that can be potentially used for this purpose.
A few of the more commonly accessible dosimeters are discussed here.

Air-filled ionization chambers

Ion chambers together with an electrometer for charge and current measurement are suited for absolute point dose calibration due to their exceptional reproducibility. The chambers need to be calibrated at NIST traceable calibration labs for the specific energies used for preclinical study. Other than radioisotopes that have constant energies, there could be a discrepancy between the X-ray energies used at the calibration lab, and the energies used for preclinical irradiation, despite the same nominal energy due to the differences in X-ray tube operational conditions, anode material, and filtration. Minimizing the HVL difference can help reduce the discrepancy. However, certain types of ion chamber, such as the Farmer chamber, respond to X-ray energies between 50 keV and 2 MeV relatively constantly, making this a manageable issue. Ion

chambers are used in many reference dosimetry protocols including AAPM TG-61[16]. The downsides of ion chambers and electrometers are that they are fragile, expensive and require a non-trivial amount of knowledge to correctly translate the reading to dose. Even with in-depth knowledge of the ion chamber calibration protocols, there could still be uncertainties translating the ion chamber readings into meaningful dose to the animals. In one of the centers surveyed by the CMCR RPC, the output was underestimated, which results in greater than expected dose, due to incorrect conversion from the air kerma to the animal dose. Another downside of ion chamber and electrometer dosimetry system is that they are impractical for in vivo measurement due to the size of the detector, high-voltage supplied to the chamber and wired nature of the setup. Ion chambers are also limited to point dose measure due to the same reasons. While ion chambers are clearly indispensable, they need to be complemented by additional dosimeters described in this chapter.

Figure 4. Farmer type ion chamber

Thermo-luminescent Detectors (TLD)

TLDs include a wide range of insulating crystals that exhibit altered crystal structure with ionizing radiation due to the electrons being released from the lattice. The release results in mobile electrons and holes that are trapped in the crystal defects in a metastable status. They are trapped until additional energy is applied to the crystal. In the case of TLD dosimetry, the crystals are heated to release the trapped carriers, which then recombine and emit visible lights. By detecting the number of visible lights using a photomultiplier tube, the ionizing radiation energy deposited on the crystal can be inferred. The most common types of TLD materials are calcium sulphate doped with dysprosium (CaSO4:Dy) or lithium flouride (LiF), both are nearly tissue equivalent, not strongly energy dependent and can be made into a wide variety of form factors that are versatile for most preclinical applications. **Figure 5** shows the energy dependence of air kerma and dose measurement using TLD for the kV X-rays relative to Co-60. TLD-100 response to the X-ray energies typically used for preclinical irradiation is within 10% of that to Co-60. TLD also stands out as one of the few reusable wireless dosimeters with consistent response up to over 1000 Gy cumulative dose. On the other hand, TLD is not easy to use as a dosimeter. Although the dosimeter itself is inexpensive, the TLD readers are costly. Moreover, typical TLD dosimeters exhibit large inter-ship variability, requiring tedious sorting process to either group TLDs with similar response, or individually calibrate and track their utilization. Yet accidental mix-up can still happen, introducing fragility and uncertainties into the TLD dosimetry system. To overcome this challenge, we recently develop a TLD fingerprinting technology for TLD-100.

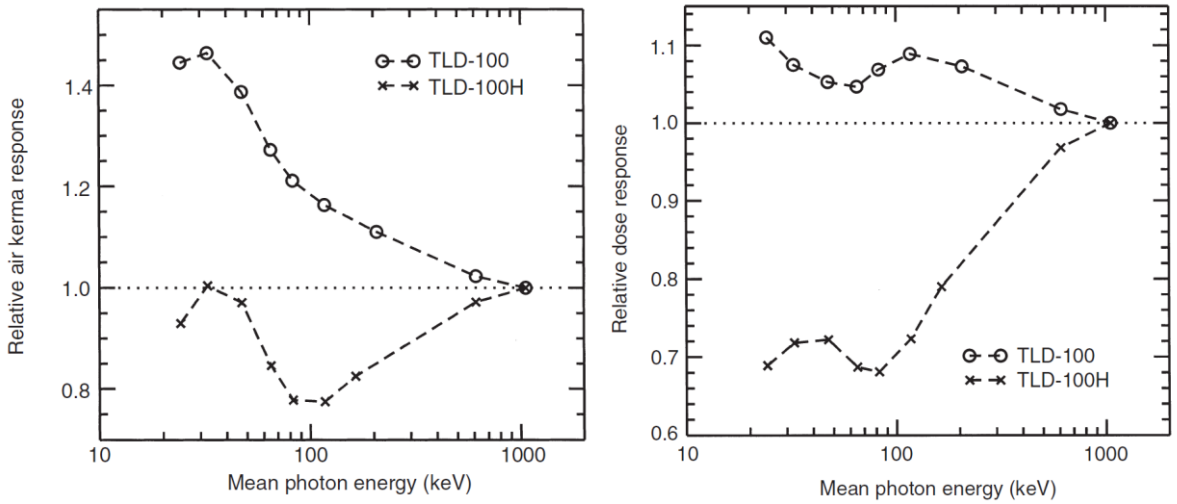

Figure 5. TLD kerma and dose response curve for lower energy X-rays calculated using the Monte Carlo and analytical method[3].

As shown in Figure 6, images of the TLD by a consumer grade USB microscope camera reveal characteristic surface texture that is unique to a specific TLD chip. The original high resolution TLD image (1600X1600) captured by a microscope camera is transformed into a 9X9 super-pixel image. The value of every super-pixel is calculated by averaging the gray level of pixels located within the super-pixel. Then, an 8-element array is computed whose elements gave a comparison of the gray level of the central super-pixel with those of its eight neighbors. Finally, the signature of an image is vectorized to have a length of 648, which is the concatenation of the 8-element arrays corresponding to the grid points, ordered left to right, top to bottom. A match is found when the distance between the signature vectors of the image to be matched and the images in the library is minimized based on cross-correlation.

The fingerprint match was repeated three times for all TLD chips. In each of the three repetitions of 752 image matches, 4, 3, and 7 images did not find a match. The single-side failure rates are thus 0.5%, 0.4%, and 0.9%, respectively. However, none of the TLDs failed both sides, resulting in a 100% success rate for chip identification. This new TLD fingerprinting method not only provides a way to individually track and inventory the TLDs and their individual calibration profiles but also is able to detect any microscopic damage to individual chips that could contribute to readout uncertainties.

The second challenge of TLD is that its results are strongly dependent on the readout and annealing processes. Although the sensitivity of individual TLDs is in principle constant within 2%, incorrect and inconsistent processes can produce highly unreliable and variable results. Therefore it is important to exactly adhere to a well-used annealing and readout protocol for TLD dosimetry, such as the one reported by Yu et al. [22] Due to this reason, trained, and more desirably, dedicated personnel is the key to the success of a TLD dosimetric program. Also due to the lengthy procedures for annealing and readout, TLDs cannot be used as a real time measurement tool.

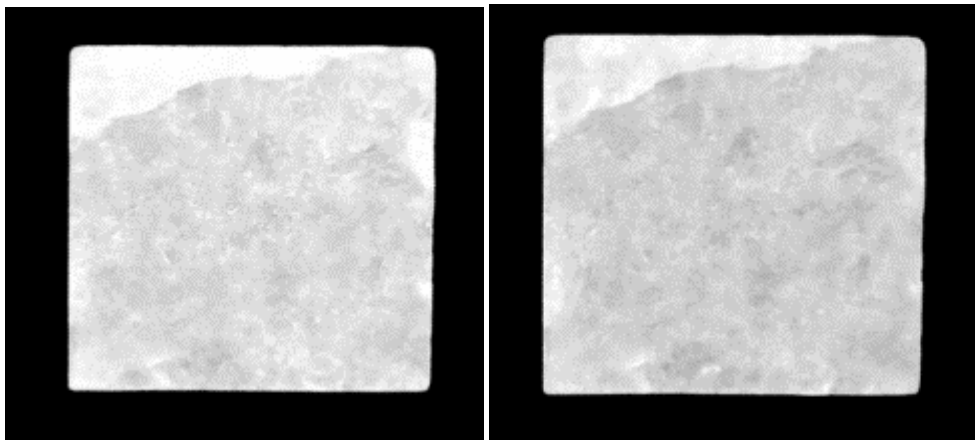

Figure 6. Two separate images of the same TLD (TLD-100, Thermofisher) showing surface features that are unique to this chip for identification. The size of the TLD chip is 3.2 mmX3.2 mmX 0.89mm.

Radiochromic film

With conventional radiographic film processors phasing out at many institutions, radiochromic films became popular for 2D

radiation dose measurement. The film contains a dye that changes color when exposed to ionizing radiation. The color change can be quantified by optical density measurement and correlated with radiation dose, allowing high-resolution 2D dose measurement. In addition to the self-developing advantage, radiochromic films are easier to cut than radiographic films into various sizes and shapes, a feature particularly desirable for preclincial dosimetry to fit into the size of the small animal phantoms. The exposed films can be digitized with relatively inexpensive flatbed scanners, such as the Epson model 10000XL, for quantitative analysis. An excellent example of using radiochromic films for preclinical irradiator dosimetry is the commissioning report of image guided confocal radiators[23], which describes the process of determining the depth dose and lateral profiles in combination with solid water slabs as shown in Figure 7.

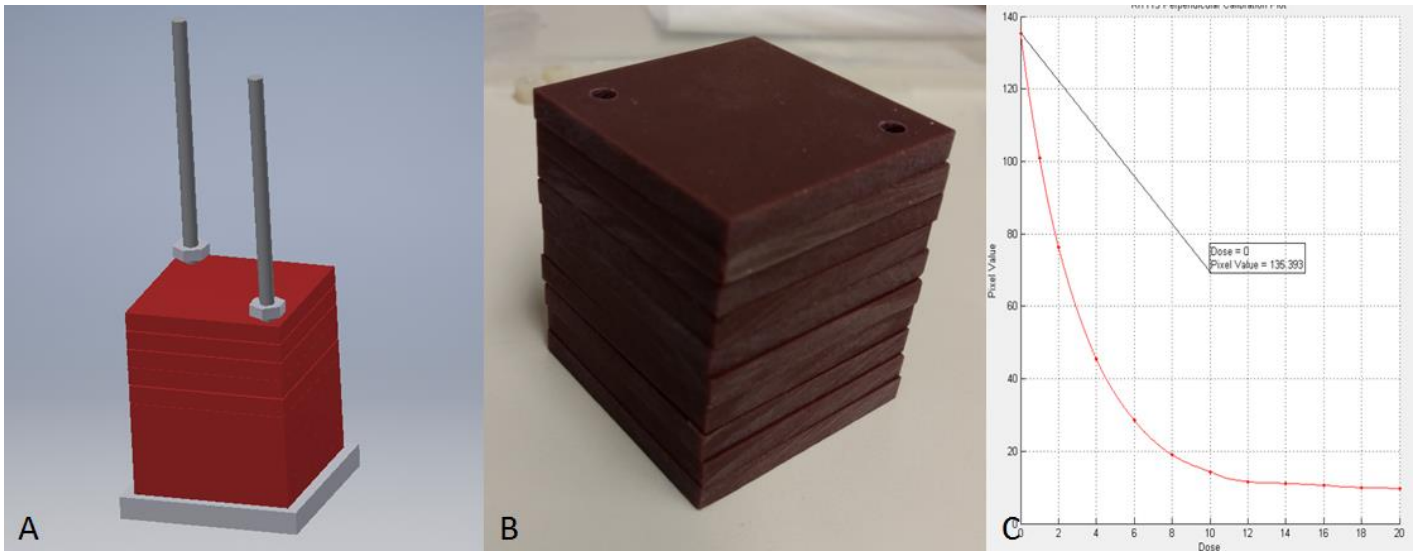

Figuer 7. A. CAD drawing of the solid water slabs. B. manufactured solid water slabs (4.5 cm squares). C. Calibration curve of the EBT3 films.

In a recent dosimetry survey performed by the UCLA CMCR Radiation Physics Core (RPC), a radiochromic film sandwiched in a mouse phantom revealed particularly high dose heterogeneity as shown in Figure 8. Instead of receiving an expected uniform dose from the dual Cs137 sources using GammaCell-40, the two ends of the mouse phantom received over 50% higher dose than the center of phantom. Investigation later revealed that the phantoms were irradiated in the standup position with the long axis of the phantom parallel to the Gamma-rays. The same set up protocol was used at this institutions for total body irradiation. As a consequence, this set up position would result in a large deviation from the intended uniform total body dose. This result clearly shows the importance of multiple point measurement or 2D measurement in these dosimetric surveys because the large unintended deviation would have not been found if only point measurement was made.

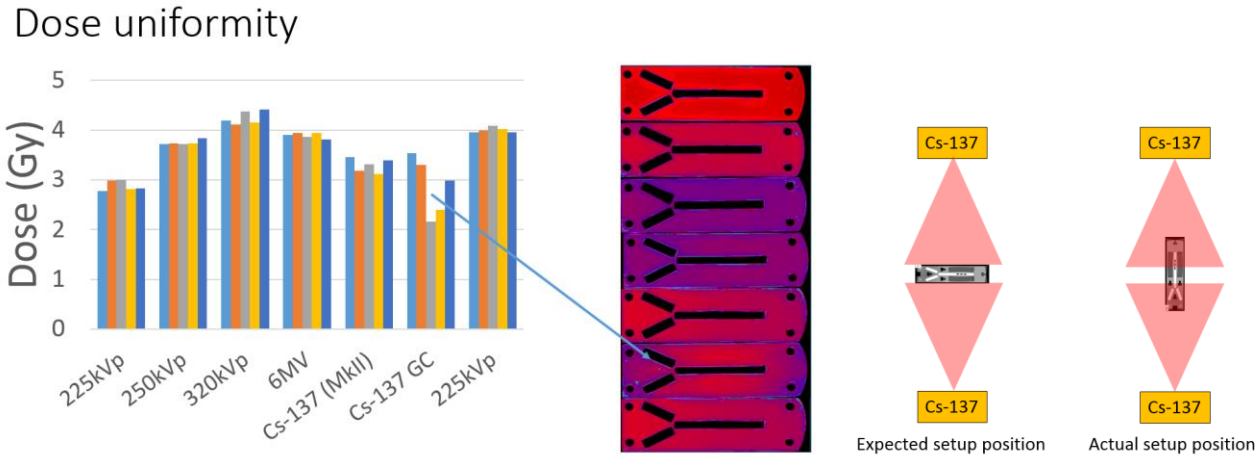

Figure 8. Field uniformity test for the 7 irradiators involved in the second survey. 5 dose readout are obtained for the head, thoracis, left and right abdomen, and pelvis of the mouse phantom using TLDs. #6 clearly shows a larger standard

deviation that can be visually correlated to the film measurement. Significantly higher dose was delivered to the head and tail of the phantom compared to the center of the phantom. Left shows the expected mouse phantom setup position and right shows the actual setup position for #6 phantom.

The weaknesses of radiochromic films are their ability to determine absolute dose. Even with careful handling of the film readout, self calibration by separate color channels[24], and optical density to dose conversion in the computer, radiochromic films exhibit substantial batch to batch variation that requires per film calibration to determine the absolute dose. As a compounding factor, radiochromic films tend to under-respond to lower energy X-rays that is evident in the kV X-ray range[25,26].

3D gel dosimetry

In cases where 2D dosimetry may be insufficient, gel dosimeters provide potentially high-resolution 3D dose measurement. Gel dosimeters contain a dye that changes color with ionizing radiation. An optical density-dose calibration curve can be established using UV-Vis spectrometer and small volume gel dosimeters exposing to known doses. The change in the 3D optical density distribution can then be digitized using an optical CT scanner[27-29]. Figure 9 shows the excellent linearity of the gel response to dose up to 35 Gy with the radiation of 225kVp X-rays.

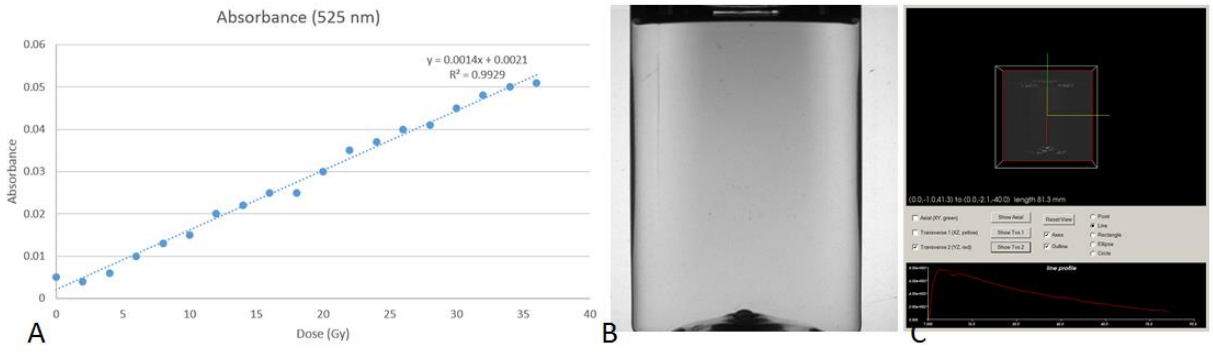

Figure 9. A. Calibration curve for the gels using UV-Vis spectrometer (GENESYS™ 10S, Thermos). B. Gel used for PDD measurement. The center of the gel is darkened by radiation. C. Percent depth dose.

The 3D gel dosimetry tool is useful to determine the volumetric dose received by the animal in total body, partial body or targeted irradiation. A powerful example of the targeted irradiation is shown in Figure 10 where two pairs of 5 mm circularly collimated orthogonal beams were projected on a 3D gel dosimeter. The 3D gel dosimeter is able to characterize the 3D dose distribution of such targeted treatments.

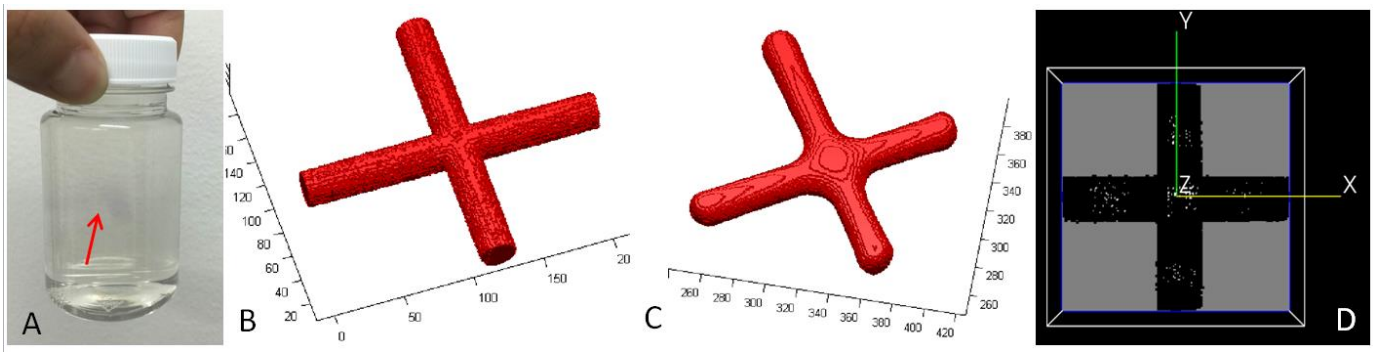

Figure 10. 3D gel dosimetry validation test. Two pairs of 5 mm circularly collimated orthogonal beams were projected on a 3D gel dosimeter. The change in optical density is visible as a purple hue in the irradiated gel bottle (A) and quantified by an optical CT scanner. After conversion to dose using a calibration curve, the measured dose (C) was compared against the calculated dose (B). (D) Gamma calculation using 2 mm/4% threshold shows a 97.5% passing rate. This unique dosimetry system allows us to validate sophisticated *3D* dose distribution.

A similar 3D dosimeter come in a different medium of plastic, which are also used for small animal dosimetry [30-35]. Similar to but more so than the radiochromic films, 3D gel dosimeter response is energy dependent and can more substantially under-respond to lower energy X-rays. 3D gel dosimeters are less commercialized and standardized than the radiochromic films in fabrication, making it even more challenging for absolute dosimetry.

OSLD dosimeter

OSLD dosimeters bear the similarity to TLDs in the production of electron and hole carriers that are trapped in crystal defects. However, different from TLDs, they can be released by light stimulation to produce visible lights, making them an interesting alternative to TLD. OSLD has been known for more than 50 years but high sensitivity OSLD such as Al2O3:C was not introduced until the 90's. Figure 8 shows a common type of OSLD nanodot enclosed in a cassette. Compared with TLDs, OSLDs have the following advantages. The process of using OSLD for dosimetry is substantially more streamlined and less dependent on operators, making it suited for general lab applications. Without involving high temperature and nitrogen gas, which are needed for TLD readout, the OSLD readers are simpler and less expensive. The light stimulation readout also allow encapsulation of individual OSLD dosimeters in a barcoded cassette for easy tracking and inventory. Moreover, unlike TLD readout that erases the stored signal, OSLD can be readout multiple times with only a small loss in signal (0.05%). The downsides of OSLD include that the dosimeter is not tissue-equivalent, it is strongly energy dependent in the kV range[36,37], and not completely reusable, meaning after 15 Gy of cumulative dose, the dosimeter response drops 5% for every 10 additional Gy[38] of dose.

Figure 11. Nanodot OSLD dosimeter and reader.

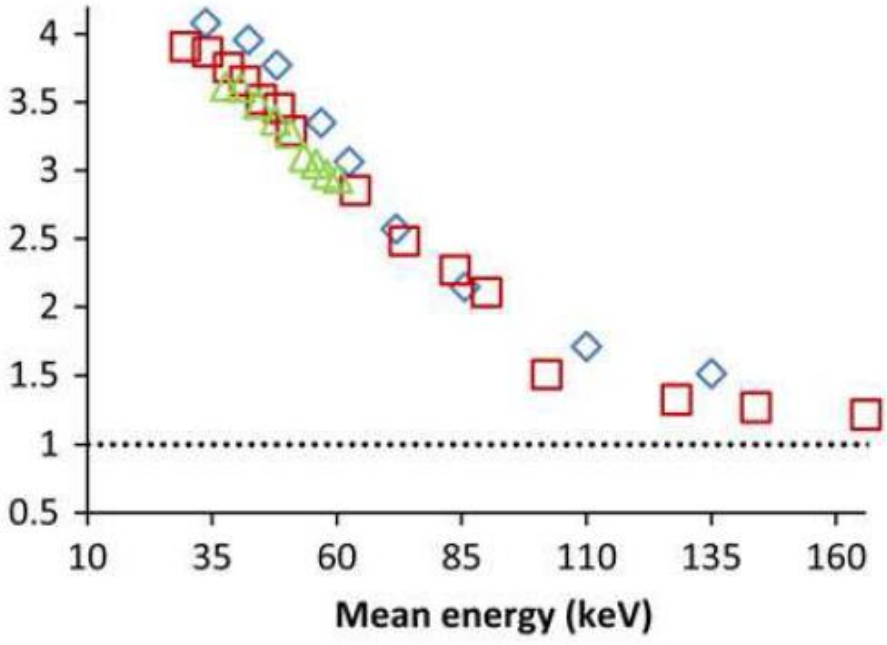

Figure 12. Nanodot OSLD response vs. effective X-ray energies[37]

Linking TG-61 with point-of-detection dosimetry

TG-61 provides a rigorous, consistent and traceable measurement of the machine output. The point-of-detection dosimeters such as TLD, OSLD and film provides a versatile measurement for the animal treatment geometry. However, thesse point-of-detection dosimeters by themselves are unreliable for absolute dose measurement without cross calibration with the air-filled air chamber measurement using TG-61. To do so, it is then important to adhere to the good beam geometry and use a field size well within the protocol specification for calibration, e.g. 10 cm or less. It is also important to provide adequate electron equilibrium by embedding these dosimeters in a phantom for dose measurement. As shown in Figure TLD has a significantly lower energy dependence for dose measurement than for air kerma measurement. Since these point-of detecters are energy dependent, the cross calibration needs to be done at every energy level that will be used for experiment.

Preclinical Phantoms

Simple geometry phantoms

In addition to dosimeters, another important element in dosimetry is the phantom, which provides the radiological environment mimicking the animals for the dosimeters. The phantoms can be approximately divided into two categories. The first category simulates the size of the animals to be studied with relatively simple, sometimes single material composition. Figure 13 shows the acrylic phantoms used in the preclinical irradiator survey and a set of commercially available mouse phantoms. Because of the simple geometry, they can be produced with high accuracy at most machine shops, allowing a way to compare dosimetry across different institutions on the same phantom geometry, without involving the time-wasting process of shipping phantoms.

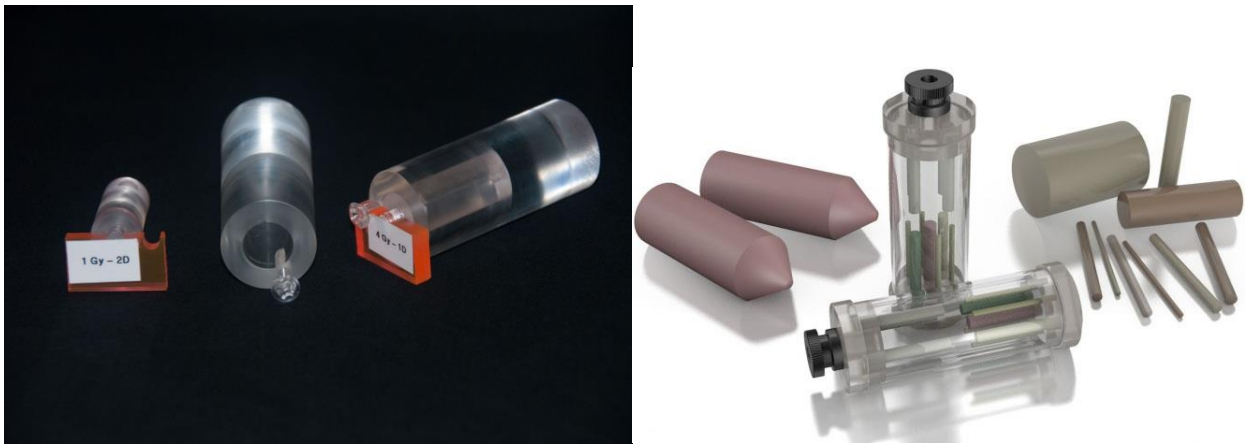

Figure 13 Simple acrylic geometry phantoms used in the previous preclinical dosimetry survey [13] and CIRS MicroMouse phantoms using the solid water material.

More recently, the CMCR RPC introduced additional tissue heterogeneity into the simple geometry phantom design to better mimic the mouse anatomy without overly complicate the manufacturing process. The phantoms are made of water mimicking polystyrene that can be separated in two halves for loading and unloading dosimeters and radiochromic films. Polystyrene's density of 1.02 g/cm^3 is closer to soft tissues than acrylic, whose density is 1.2 g/cm^3. Each phantom also comes with lung (0.3 g/cm^3 Polyurethane rod, McMaster-Carr) and bone inserts (Teflon rod, 2.2g/cm^3) that will be valuable to determine dose to these lower and higher density tissues. A CT of the mouse phantom is shown in **Figure 3**. There are 15 TLD in triplets slots to report dose to the head, chest, abdomen, and pelvis. Six additional TLD can be fit into both sides of the lung. In addition to the point dose measurement, radiochromic films are cut using a digital film cutter (Silver Bullet) for the phantom for 2D dosimetry.

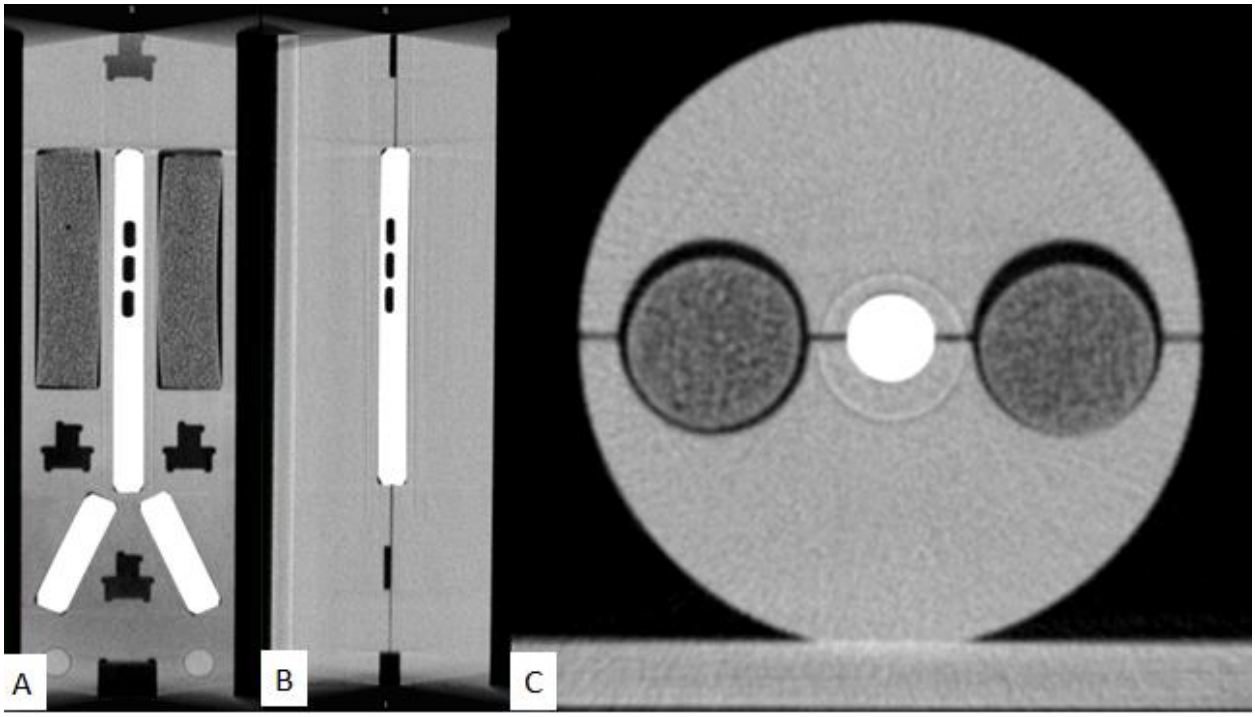

Figure 14. CT of the production phantom showing bone and lung inserts. There are 5 TLD locations each with 3 slots for TLD dosimetry.

Phantoms minicking the actual animal shape and tissue heterogeneity

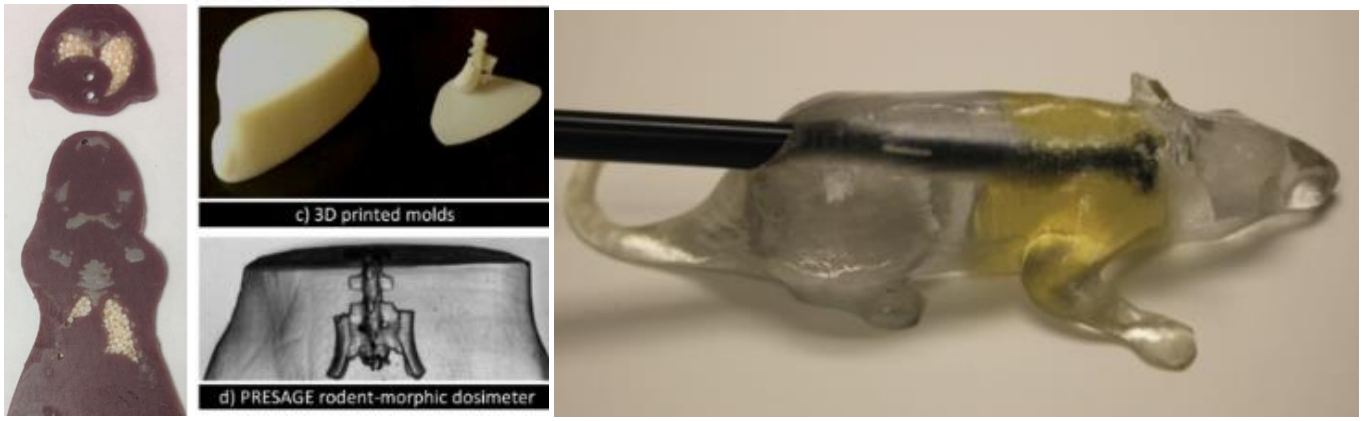

Figure 14. From left to right, a slice of mouse phantom constructed based on segmented CT scan data[39], integrated 3D presage dosimeter with anatomically accurate rodent-morphic phantom[34], and a 3D printed anthropomorphic phantom for linear accelerator-based small animal irradiaton with a hole for ion-chamber[40].

Geometry phantoms can be made with the dimension similar to the animal to be studied. However, they are not a high fidelity representation of the animal anatomies and morphology. There have been several publications reporting the mousemorphic phantoms that more closely mimic the animal tissue and morphological properties. Figure 14 shows three representative work. Each of these phantoms has their unique features that are suited for certain dosimetric tests. The phantom shown in the left [39] uses highly tissue relevant materials for the soft tissues, lungs, and bones. The slice by slice construction is compatible with the need for film dosimetry. The phantom in the middle uses Presage 3D dosimeter for soft tissue. Similar to the gel dosimeter, Presage 3D dosimeter contains a dye that changes color with ionizing radiation and the change can be mapped using an optical CT scanner [34]. The phantom on the right [40] represents a new way of making animal mimicking phantoms using 3D printing technology, which has a tremendous growth in printing quality and material selection in the past 10 years. One potential challenge of using these more sophisticated phantoms is that they are difficult and costly to make. Different from the simple geometry phantoms, reproducing these phantoms with high accuracy is not trivial. Some of the complex phantoms, such as the 3D Presage phantoms are meant to be single use due to the irreversible

changes in optical density by ionizing radiation. However, with 3D printing technology, the cost and complexity of making animal-mimicking phantoms are substantially reduced.

As part of the CMCR dosimetric project, a mousemorphic phantom was developed based on micro CT of a C57Bl/6 mouse. The mousemorphic phantom has two configurations shown in **Figure 15** for TLD and OSLD, respectively. The phantom was printed using a 3D printer (MakerGear M2 Desktop 3D Printer) and Acrylonitrile Butadiene Styrene (ABS) filament that has a density of 1.04g/cm^3, which is nearly tissue equivalent[41]. Initial dosimetric calibration was performed using a 225kVp X-ray machine with Monte Carlo dose calculation. By assuming ABS tissue equivalent in Monte Carlo simulation, the measured dose was 1.2% off from the calculated dose, showing that ABS mousemorphic phantoms are good surrogates for dosimetric tests. Inter-phantom variation is assessed by their weight showing less than 0.5% variation.

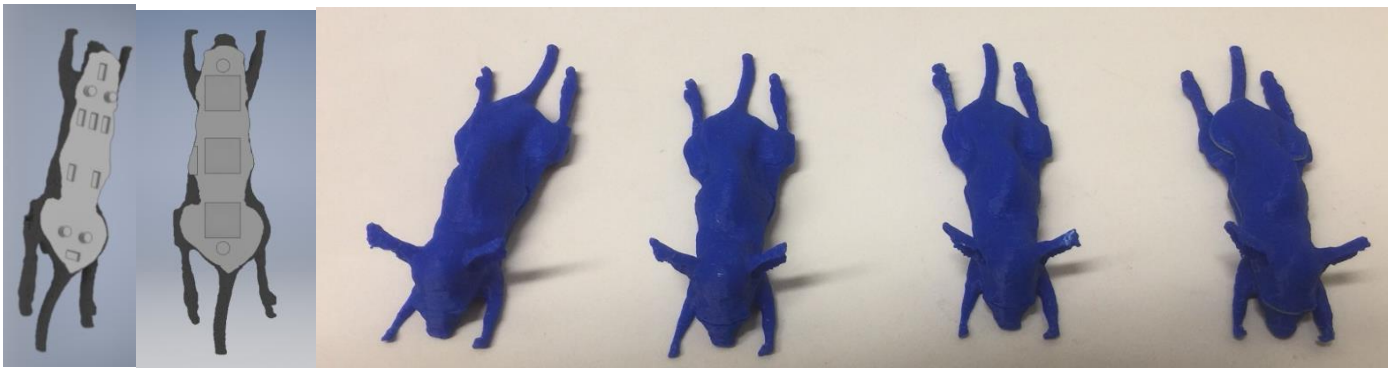

Figure 15. (Top row) the CAD design of the mousemorphic phantom. The first version is for embedded TLD-100 chips and the second version is for embedded OSLD chips. (Bottom row) the actual 3D printed phantoms based on the CAD design. The weight of the phantom is 24.5 ±0.1g.

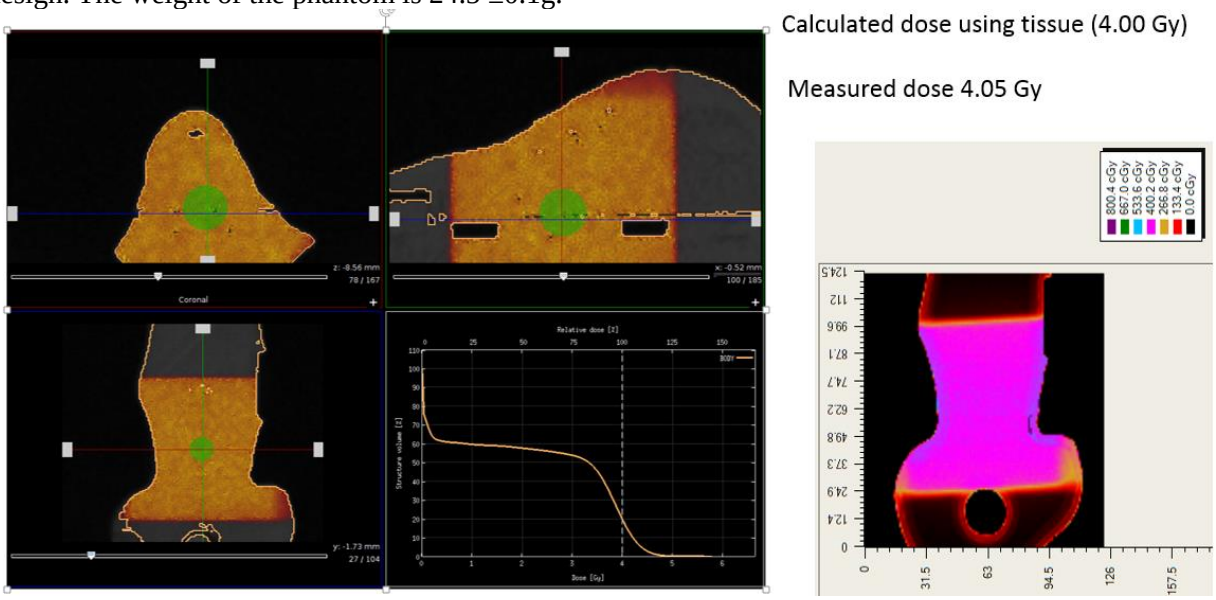

Figure 16. (Right) Monte Carlo dose calculation on the mousemorphic phantom assuming tissue equivalent material. (Left) Measured dose using film and OLSD.

Dosimetric harmonization by CMCR RPC

With the amount of available dosimetric tools and dosimetric surveys showing potential discrepant dosimetry at different preclinical facilities, an important question to ask is whether harmonization in dosimetry is possible. After performing remote dosimetry survey similar to that of [13]. The results are shown in Figure 17. The survey was first repeated to assess the reproducibility of the dosimetric measurement to deliver 4 Gy to the cylindrical phantom shown in Figure 14. Similar to what was reported in [13], large deviations up to 30% from the expected dose is observed. After comparing the measured dose with the expected dose, the change to the exposure time is communicated to the participating centers for the third batch of irradiation.

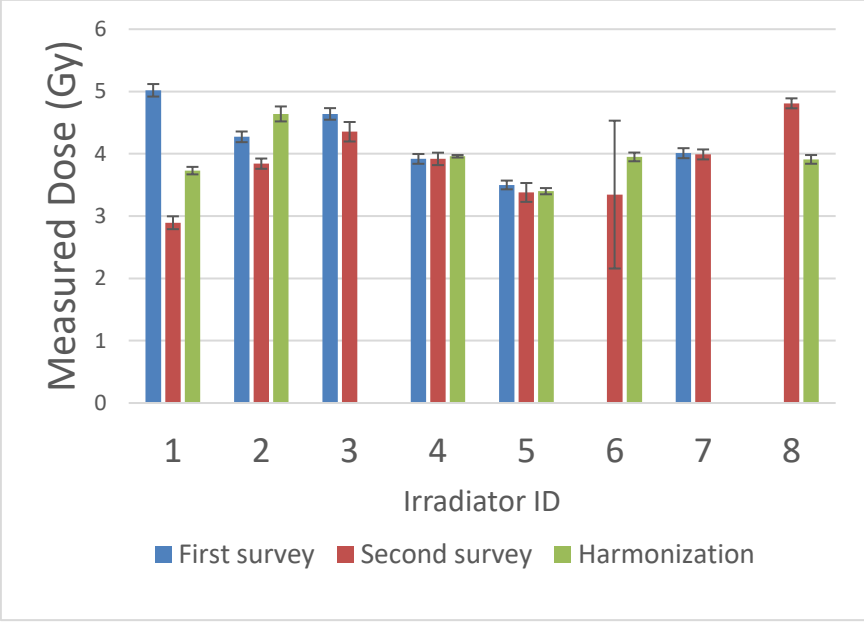

Figure 17. Harmonization tests results. Irradiator #6 and #8 did not participate the first survey, harmonization result of irradiator #3 was invalid. The exposure parameter for irradiator #5 was not adjusted.

All except one center were able to improve the dosimetric deviation from the expected value to within 7%. The single center that shows persistent dosimetric deviation later realized that they did not adjust their exposure according to the revised instruction. On the other hand, the center is now aware of the consistent deviation and will make future adjustment accordingly. It is worth noting that the large dose heterogeneity at #6 due to improper animal set up is improved in the harmonization test to be within 2%. At the same time, the absolute dose error is reduced to 1% at the same time.

Conclusion

The chapter outlines challenges and opportunities to improve the consistency of one specific link in the preclinical radiobiology study, which is to quantify the dose delivered to the animal. This is clearly a complicated topic involving physics, engineering, and biology. Successful collaboration between these specialties is clearly critical to the dosimetric accuracy. Other than the limited resource to foster such collaboration, a more often obstacle is the lack of communication between specialties. Irradiators are often assumed as push-button instruments that are expected to deliver the dose that is dialed into the control panel. Physics and engineer involvement is needed only when the machines are clearly malfunctioning and in need of repair. Hopefully, the chapter provides an overview of the intricate physics dosimetry, the amount of technology that is potentially available, and the consequence without accurate radiation dosimetry, e.g. large deviation from the intended dose that can potentially invalidate the entire study. In addition to the absolute point dose calibration emphasized in the chapter, the importance of more intimately involving physics in biology study design is as follows.

In addition to the dosimetric harmonization test, CMCR RPC also provided custom dosimetric service for partial body irradiation. An example is shown below in Figure 18 where the 3D printed mousemorphic phantom shown in Figure 15 was irradiated with lead blocks to protect the head and rear legs from irradiation. Consistent to the film readings, the TLD showed 3.88 Gy (expected dose 4.00 Gy) to the exposed volume and 1.61 Gy to the protected volumes, which is 41% of the open area. The shielded volume dose was significantly higher than the 10% expected by the PI. Additional lead shielding is thus needed to achieve the goal.

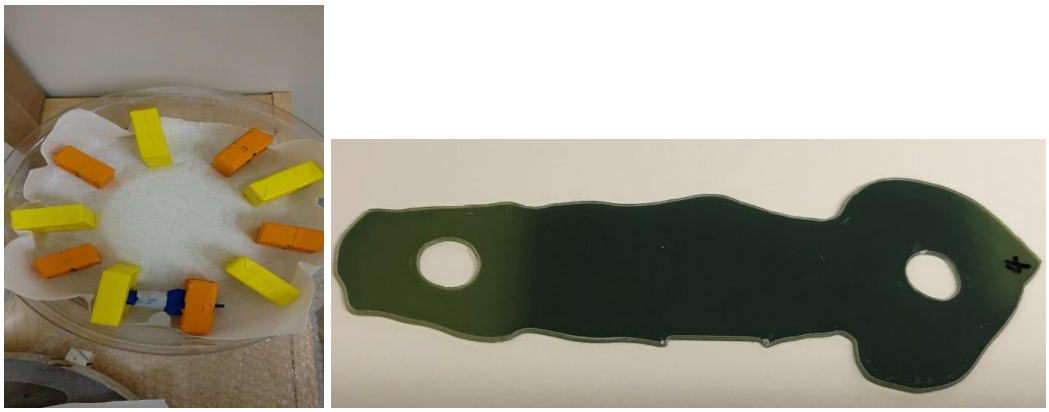

Figure 18. Custom partial body dosimetry. (left) experimental set up. (right) film measurement.

Therefore, the chapter strongly echoes the recommendations made by the NCI, NIAID and NIST workshop. Specifically, biologists and physicists should collaborate on study design and execution. A robust mechanism needs to be in place to ensure such collaboration. An encouraging example of such mechanism is a recent funding opportunity for Cooperative Agreement to Develop Targeted Agents for Use with Systemic Agents Plus Radiotherapy. The full announcement can be read at https://grants.nih.gov/grants/guide/pa-files/PAR-16-111.html, in which, a minimum budget and technical requirement for the physics dosimetry is specified for qualified applications. Unfortunately, despite the many types of dosimeters that are available, they all have deficiencies preventing them from the ideal solution for preclinical dosimetry. There is still not a straightforward way to quickly determine the beam quality. Therefore, there is an urgent need to encourage technological innovations that provide accurate, fast, inexpensive and easy to use dosimetric tools.

In addition to the inclusion of the physicists at individual institutions and standard operational procedures, an intercomparison program by one or more groups seems to be essential to the harmonization of dosimetry. Due to the huge variation in experience and technology at many preclinical irradiation facilities, the centralized organization, much like IROC for human irradiation, is the only way to independently verify the dosimetry[42]. The service can grow from existing infrastructures related to national calibration labs and the radiation physics cores that are currently funded to support various biology programs.

This chapter provides a snapshot of preclinical physics dosimetry. Important physics quantities such as the dose delivery time[43,44] is not included despite its potential importance to the tissue damage and repair. Different from the radiation dose, the treatment time is more straightforward to measure, but may not be practical to harmonize due to variations in machine output and variations in experimental setup. This additional level of complexity warrants a separate document to discuss.

Acknowledgment

This work is supported in part by NIAID for grant support (U19AI067769 sub-project ID: 5126 Radiation Physics Core). Dr. Sheng would like to thank Drs. Guy Garty, Michael Epperly, Terry Yoshizumi, J. Daniel Bourland, June Brickey, Evagelia (Lia) Laiakis and Keisuke Iwamoto for their help in performing the RPC dosimetric tasks.

References:

1. Alberts B, Kirschner MW, Tilghman S, Varmus H (2014) Rescuing US biomedical research from its systemic flaws. Proc Natl Acad Sci U S A 111: 5773-5777.
2. Errington TM, Iorns E, Gunn W, Tan FE, Lomax J, et al. (2014) An open investigation of the reproducibility of cancer biology research. Elife 3.
3. Nunn AA, Davis SD, Micka JA, DeWerd LA (2008) LiF : Mg,Ti TLD response as a function of photon energy for moderately filtered x-ray spectra in the range of 20-250 kVp relative to Co-60. Medical Physics 35: 1859-1869.
4. Begley CG, Ellis LM (2012) Drug development: Raise standards for preclinical cancer research. Nature 483: 531-533.
5. Nosek BA, Errington TM (2017) Making sense of replications. Elife 6.
6. Freedman LP, Cockburn IM, Simcoe TS (2015) The Economics of Reproducibility in Preclinical Research. PLoS Biol 13: e1002165.
7. Yu J, Straube W, Mayo C, Giaddui T, Bosch W, et al. (2014) Radiation therapy digital data submission process for national clinical trials network. Int J Radiat Oncol Biol Phys 90: 466-467.
8. Nwankwo O, Mekdash H, Sihono DS, Wenz F, Glatting G (2015) Knowledge-based radiation therapy (KBRT) treatment planning versus planning by experts: validation of a KBRT algorithm for prostate cancer treatment planning. Radiat Oncol 10: 111.
9. Good D, Lo J, Lee WR, Wu QJ, Yin FF, et al. (2013) A knowledge-based approach to improving and homogenizing intensity modulated radiation therapy planning quality among treatment centers: an example application to prostate cancer planning. Int J Radiat Oncol Biol Phys 87: 176-181.
10. Chow JC, Leung MK, Lindsay PE, Jaffray DA (2010) Dosimetric variation due to the photon beam energy in the small-animal irradiation: a Monte Carlo study. Med Phys 37: 5322-5329.
11. Desrosiers M, DeWerd L, Deye J, Lindsay P, Murphy MK, et al. (2013) The Importance of Dosimetry Standardization in Radiobiology. J Res Natl Inst Stand Technol 118: 403-418.
12. Brenner DJ, Chao NJ, Greenberger JS, Guha C, McBride WH, et al. (2015) Are We Ready for a Radiological Terrorist Attack Yet? Report From the Centers for Medical Countermeasures Against Radiation Network. Int J Radiat Oncol Biol Phys 92: 504-505.
13. Pedersen KH, Kunugi KA, Hammer CG, Culberson WS, DeWerd LA (2016) Radiation Biology Irradiator Dose Verification Survey. Radiat Res 185: 163-168.
14. Brodin NP, Chen Y, Yaparpalvi R, Guha C, Tome WA (2016) Dosimetry Formalism and Implementation of a Homogenous Irradiation Protocol to Improve the Accuracy of Small Animal Whole-Body Irradiation Using a 137Cs Irradiator. Health Phys 110: S26-38.
15. Yoshizumi T, Brady SL, Robbins ME, Bourland JD (2011) Specific issues in small animal dosimetry and irradiator calibration. Int J Radiat Biol 87: 1001-1010.
16. Ma CM, Coffey CW, DeWerd LA, Liu C, Nath R, et al. (2001) AAPM protocol for 40-300 kV x-ray beam dosimetry in radiotherapy and radiobiology. Med Phys 28: 868-893.
17. Brady SL, Toncheva G, Dewhirst MW, Yoshizumi TT (2009) Characterization of a 137Cs irradiator from a new perspective with modern dosimetric tools. Health Phys 97: 195-205.
18. American_National_Standards_Institute (1978) American National Standard Procedures for Periodic Inspection of Cobalt-60 and Cesium-137 Teletherapy Equipment. ANSI N449.
19. Pelisser A, Vier-Pelisser F, Fontanella V, de Figueiredo M (2007) Microscopical analysis of fractionated cobalt-60 radiotherapy effects on mandibles of rats. Radiol Bras 40: 113-118.
20. Moore G, Pomper M (2015) A Roadmap for Replacing High-Risk Radioactive Sources and Materials https://wwwnonproliferationorg/wp-content/uploads/2015/07/permanent_risk_reductionpdf.
21. A B, IM I (2018) California's Radiological Threat Reduction Initiative. Institute for Nuclear Materials Management (INMM) 59 Annual Meeting.
22. Yu C, Luxton G (1999) TLD dose measurement: a simplified accurate technique for the dose range from 0.5 cGy to 1000 cGy. Med Phys 26: 1010-1016.
23. Tryggestad E, Armour M, Iordachita I, Verhaegen F, Wong JW (2009) A comprehensive system for dosimetric commissioning and Monte Carlo validation for the small animal radiation research platform. Phys Med Biol 54: 5341-5357.
24. Mathot M, Sobczak S, Hoornaert MT (2014) Gafchromic film dosimetry: Four years experience using FilmQA Pro software and Epson flatbed scanners. Physica Medica-European Journal of Medical Physics 30: 871-877.

25. Villarreal-Barajas JE, Khan RF (2014) Energy response of EBT3 radiochromic films: implications for dosimetry in kilovoltage range. J Appl Clin Med Phys 15: 4439.
26. Chiu-Tsao S, Massillon-JL G, Domingo-Munoz IDM, Chan M (2012) Energy Dependence of the New GafChromic-EBT3 Film's Dose Response-Curve. Medical Physics 39: 3724-3724.
27. Colnot J, Huet C, Gschwind R, Clairand I (2018) Characterisation of two new radiochromic gel dosimeters TruView and ClearView in combination with the vista optical CT scanner: A feasibility study. Phys Med 52: 154-164.
28. Olding T, Schreiner LJ (2011) Cone-beam optical computed tomography for gel dosimetry II: imaging protocols. Phys Med Biol 56: 1259-1279.
29. Babic S, Battista J, Jordan K (2008) Sci-Fri PM: Planning-07: A low diffusion radiochromic gel dosimeter for three-dimensional radiation dosimetry. Med Phys 35: 3413.
30. Na YH, Wang YF, Black PJ, Velten C, Qian X, et al. (2018) Dosimetric and geometric characteristics of a small animal image-guided irradiator using 3D dosimetry/optical CT scanner. Med Phys 45: 3330-3339.
31. Yoon SW, Cramer CK, Miles DA, Reinsvold MH, Joo KM, et al. (2017) A precision 3D conformal treatment technique in rats: Application to whole-brain radiotherapy with hippocampal avoidance. Med Phys 44: 6008-6017.
32. Pelliccia D, Poole CM, Livingstone J, Stevenson AW, Smyth LM, et al. (2016) Image guidance protocol for synchrotron microbeam radiation therapy. J Synchrotron Radiat 23: 566-573.
33. Gagliardi FM, Cornelius I, Blencowe A, Franich RD, Geso M (2015) High resolution 3D imaging of synchrotron generated microbeams. Med Phys 42: 6973-6986.
34. Bache ST, Juang T, Belley MD, Koontz BF, Adamovics J, et al. (2015) Investigating the accuracy of microstereotactic-body-radiotherapy utilizing anatomically accurate 3D printed rodent-morphic dosimeters. Med Phys 42: 846-855.
35. Newton J, Oldham M, Thomas A, Li Y, Adamovics J, et al. (2011) Commissioning a small-field biological irradiator using point, 2D, and 3D dosimetry techniques. Med Phys 38: 6754-6762.
36. Reft CS (2009) The energy dependence and dose response of a commercial optically stimulated luminescent detector for kilovoltage photon, megavoltage photon, and electron, proton, and carbon beams. Med Phys 36: 1690-1699.
37. Poirier Y, Kuznetsova S, Villarreal-Barajas JE (2018) Characterization of nanoDot optically stimulated luminescence detectors and high-sensitivity MCP-N thermoluminescent detectors in the 40-300 kVp energy range. Med Phys 45: 402-413.
38. Jursinic PA (2010) Changes in optically stimulated luminescent dosimeter (OSLD) dosimetric characteristics with accumulated dose. Med Phys 37: 132-140.
39. Welch D, Harken AD, Randers-Pehrson G, Brenner DJ (2015) Construction of mouse phantoms from segmented CT scan data for radiation dosimetry studies. Phys Med Biol 60: 3589-3598.
40. Perks JR, Lucero S, Monjazeb AM, Li JJ (2015) Anthropomorphic Phantoms for Confirmation of Linear Accelerator-Based Small Animal Irradiation. Cureus 7: e254.
41. Kairn T, Crowe S, Markwell T (2015) Use of 3D Printed Materials as Tissue-Equivalent Phantoms. World Congress on Medical Physics and Biomedical Engineering 51: 728-731.
42. van der Merwe D, Van Dyk J, Healy B, Zubizarreta E, Izewska J, et al. (2017) Accuracy requirements and uncertainties in radiotherapy: a report of the International Atomic Energy Agency. Acta Oncol 56: 1-6.
43. Moiseenko V, Banath JP, Duzenli C, Olive PL (2008) Effect of prolonging radiation delivery time on retention of gammaH2AX. Radiat Oncol 3: 18.
44. Yang W, Wang L, Larner J, Read P, Benedict S, et al. (2009) Tumor cell survival dependence on helical tomotherapy, continuous arc and segmented dose delivery. Phys Med Biol 54: 6635-6643.